 Bull. Chem. Soc. Jpn., **76**, 59–71 (2003)

An Extended Fano–DeVoe Polarizability Theory Similar to the Bayley–Nielsen–Schellman Secular Matrix Method: CD Calculations of Polypeptides Having α-Helix, β-Sheet, and β-Turn Structures

Hirotoshi Ito

Department of Applied Physics and Chemistry, The University of Electro-Communications, 1-5-1 Chofugaoka, Chofu, Tokyo 182

(Received December 19, 2001)

We have expanded the previous Bayley–Nielsen–Schellman type polarizability theory so as to involve a new diagonal type of *CAE* (Condon, Alter, Eyring) interaction energy as {(the previous diagonal type of *CAE* interaction energy) − (the electrostatically corrected ground state energy)}, which corresponds to the term pointed out by Misra in his review article. For the CD and UV band shape functions which were previously derived in a different way, we have newly rederived the polymer CD and UV band shape functions by making use of the Green's function method, starting from the well-known text book by Eyring et al. For a monomer polarizability tensor, the two most often used Lorentzian and Gaussian band approximations will be studied together with practically necessary relationships on the bandwidths.

The theory has been applied to the CD and UV absorption calculations on polypeptides. Previously, unless one scaled the earlier diagonal type of *CAE* interaction energy, poor predictions were then obtained, especially for the β-sheet polypeptides as well as the small α-helix and β-turn tripeptides. Now, using the new diagonal type of *CAE* interaction energies, promising CD results have been obtained together with reasonable UV spectral shifts.

We have recently developed an extended Fano–DeVoe polarizability tensor theory for circular dichroism (CD) and ultraviolet (UV) and visible absorption spectra.[1] This extended theory has been formulated in terms of a Bayley–Nielsen–Schellman-type model Hamiltonian,[2] which involves the original Fano–DeVoe type of inter(sub)molecular interaction energies[3] and the *off-diagonal* types of *CAE* (Condon, Altar, Eyring) *one-electron* electrostatic interaction energies;[4] to such a Hamiltonian, we have further added the *diagonal* types of *CAE* interaction energies which are essentially necessary.

So far, similar kinds of Bayley–Nielsen–Schellman-type secular matrix method[2,5–7] have successfully been applied to the CD spectra for polypeptides. The successes might be brought about by the fact that only the *diagonal* type of *CAE* interaction energies have wisely been dropped. The previously extended polarizability theory[1] has been able to predict well the CD and UV absorption spectra for the long α-helix polypeptides using the CNDO/S monomer properties.[8–10] However, the theory has poorly predicted those spectra not only for the small α-helix and β-turn tripeptides, but also for β-sheet polypeptides. For predicting well these CD and UV spectra, the previously extended theory has required us to scale down the diagonal type of *CAE* interaction energies; otherwise, extraordinarily large spectral shifts were numerically observed. This indicates that the overestimation of the diagonal energies sensitively depends upon the peptide back-bone geometries of these conformations.

To refine the theory, we have found it necessary to modify the previously extended Fano–DeVoe Hamiltonian,[1] so as to involve a new diagonal type of *CAE* interaction energy such as {(the previous diagonal type of *CAE* interaction energy) − (the electrostatically corrected ground state energy)}. This *CAE* interaction energy is similar to the diagonal one for the secular equation pointed out by Misra,[11] who discussed the influence of the permanent dipole moments on the electronic spectra of molecular crystals.

In section 1 of the theoretical part, we derive a newly extended Fano–DeVoe Hamiltonian closely along with the treatment suggested by Misra[11] as well as with the description of the excitation-energy operator presented by Davydov[12] and Kopelman.[13] In section 2, on the basis of such a new Hamiltonian, we briefly outline the polymer polarizability tensors. Recently, we have extended the first-order-*dimer* model for predicting the CD band shape function presented by Stiles and Buckingham[14,15] to an infinite-order *N-mer* model.[1,16] However, in section 3, starting from the well-known textbook by Eyring et al.,[17] we make use of Green's function method to rederive newly the CD band shape function. In section 4, for the imaginary and real parts of a monomer polarizability tensor, the two most often used Lorentzian and Gaussian band approximations will be discussed. Finally, the present method is applied to the CD and UV absorption band shape calculations not only on polypeptides having α-helix and β-sheet structures, but also on a type II β-turn tripeptide such as *N*-acetyl-Pro-Gly-Leu-OH. The present formulation has led to promisingly improved CD spectra and the reasonable UV spectral shifts.

Theoretical

1. Extended Fano–DeVoe Hamiltonian. It may be convenient for a polymer (*N*-mer) to divide the total Hamiltonian

$\mathscr{H}$ as follows :

$$\mathscr{H} = \sum_{m=1}^{N} H_0^{(m)} + \sum_{m=1}^{N}\sum_{n>m}^{N} V_{mn} \equiv H_0 + V, \quad (1)$$

where $H_0^{(m)}$ represents the Hamiltonian of an mth monomer. V_{mn} signifies the inter(sub)molecular Coulomb interaction operators, for which we make use of the dipole approximation. The monomer spectroscopic parameters involving the excitation energies and the transition moments are sometimes assumed to be experimentally known;[3] theoretically these are determined by the secular equation for $H_0^{(m)}$ in the configuration interaction (CI) method.[1,18,19]

Closely following Davydov's description[12] for the Frenkel tight binding approximation, we signify the total ground state $|0>$ by the product $|\Pi_k^N \Phi_0^{(k)}>$ of the monomer ground states $\Phi_0^{(m)}$ for $H_0^{(m)}$. When $\Phi_f^{(m)}$ is an fth excited state $\Phi_f^{(m)}$ of the mth monomer, each one-site excited state $|fm>$ is expressed by $|\Phi_f^{(m)} \Pi_{k\neq m}^N \Phi_0^{(k)}>$. The λth exciton states $|\lambda>$ of the polymer (λ = 1, 2, 3, ...) are then expanded in terms of the one-site excited states $|fm>$ as

$$|\lambda> = \sum_{m=1}^{N}\sum_{f\neq 0}^{levels} C_{fm}^{\lambda}|fm> = \sum_{m=1}^{N}\sum_{f\neq 0} <fm|\lambda>|fm>. \quad (2)$$

In this limited subspace spanned by the one-site excited states $|fm>$, the completeness such as $\sum_{m=1}^{N}\sum_{f\neq 0}|fm><fm| = 1$ is assumed.

A matrix representation of Eq. 1, *explicitly* relative to the total ground state energy E_0 ($= <0|\mathscr{H}|0>$), can be written as follows:[12,13]

$$\begin{aligned} H &= \mathscr{H} - E_0 \\ &= \sum_{m=1}^{N}\sum_{f\neq 0}\sum_{n=1}^{N}\sum_{g\neq 0}|fm><fm|\mathscr{H}|gn><gn| - <0|\mathscr{H}|0> \\ &= \sum_{m=1}^{N}\sum_{f\neq 0}|fm>(<fm|H_0|fm> - <0|H_0|0>)<fm| \\ &\quad + \sum_{m=1}^{N}\sum_{f\neq 0}|fm>(<fm|V|fm> - <0|V|0>)<fm| \\ &\quad + \sum_{m=1}^{N}\sum_{f\neq 0}\sum_{g\neq 0;\, g\neq f}|fm><fm|V|gm><gm| \\ &\quad + \sum_{m=1}^{N}\sum_{f\neq 0}\sum_{n\neq m}^{N}\sum_{g\neq 0}|fm><fm|V|gn><gn|, \end{aligned} \quad (3)$$

One may realize that this Hamiltonian is similat to the excitation energy operators in Davydov's book[12] and also in Kopelman's article.[13] It is to be noted that in Ref. 12 the electrostatic effect $<0|V|0>$ in the first order of $\mathscr{H}$ was taken into account in Eqs.(3.6) and (3.6a) of Chapter II as well as in Eq.(2.20) of the Hamiltonian operator in Chapter III. However, Misra had already pointed out that this substraction of $<0|V|0>$ from the secular equations for molecular crystals is necessary.[11] Usually, $<0|\mathscr{H}|0>$ may be taken to be implicitly zero as a reference energy $<0|H_0|0>$ in the zeroth order. If there exist some permanent dipole moments, we must consider the first-order energies $<0|V|0>$ pointed out by Misra[11] with relation to the calculations of $<fm|V|fm>$ mentioned below.

In regard to the diagonal m, f, m, f-terms of Eq. 3, we have mth site excitation energies:

$$<fm|H_0|fm> - <0|H_0|0> = \hbar\,\omega_{f0}^{(m)}, \quad (4)$$

where $\omega_{f0}^{(m)} = E_{f0}^{(m)}/\hbar$. For the previous diagonal type of *CAE* energy V_{mm}^{ff},[1] the new diagonal type of electrostatic energy V_{mm}^{ff} is given by

$$\begin{aligned} &<fm|V|fm> - <0|V|0> \\ &\equiv V_{mm}^{ff} = \sum_{k\neq m}^{N} \boldsymbol{\mu}_{ff}^{(m)} \cdot \boldsymbol{U}_{mk}^{ff,0} \cdot \boldsymbol{\mu}_{00}^{(k)} - \sum_{k\neq m}^{N} \boldsymbol{\mu}_{00}^{(m)} \cdot \boldsymbol{U}_{mk}^{00,00} \cdot \boldsymbol{\mu}_{00}^{(k)}, \end{aligned} \quad (5)$$

where $\Sigma_{n\neq m}\Sigma_{j\neq n,m}\boldsymbol{\mu}_{00}^{(n)} \cdot \boldsymbol{U}_{nj}^{00,00} \cdot \boldsymbol{\mu}_{00}^{(j)}/2$ involved in the two terms are canceled out. Equation 5 was just referred to by Misra.[11] In Ref. 1, the second term of the right-hand side of Eq. 5 has been dropped. The unit dipole interaction tensors between distances $|\boldsymbol{R}_k^{00} - \boldsymbol{R}_m^{ff}| \equiv |\boldsymbol{R}_{mk}^{ff,00}|$ are denoted by :

$$\boldsymbol{U}_{mk}^{ff,00} = [|\boldsymbol{R}_{mk}^{ff,00}|^2\mathbf{1} - 3\boldsymbol{R}_{mk}^{ff,00}\boldsymbol{R}_{mk}^{ff,00}]|\boldsymbol{R}_{mk}^{ff,00}|^{-5}, \quad (6)$$

and $\boldsymbol{U}_{mk}^{00,00}$ is similarly defined. $\boldsymbol{\mu}_{ff}^{(m)}$ denotes an fth excited dipole moment of an mth monomer at the location $\boldsymbol{R}_m^{ff}$, and $\boldsymbol{\mu}_{00}^{(k)}$ represents the permanent dipole moment at a kth position $\boldsymbol{R}_k^{00}$. Bayley et al.[2] ignored the diagonal type of *CAE* interaction energies V_{mm}^{ff}, but they took into account the off-diagonal type of *CAE* energies $V_{mm}^{fg} \equiv <fm|V|gm>$ in addition to the genuine Fano-DeVoe type of interaction energies[3] $V_{mm}^{fg} \equiv <fm|V|gn>$ between distances $|\boldsymbol{R}_n^g - \boldsymbol{R}_m^f| \equiv |\boldsymbol{R}_{mn}^{fg}|$, which are calculated by $\boldsymbol{\mu}_{f0}^{(m)} \cdot \boldsymbol{U}_{mn}^{f0,0g} \cdot \boldsymbol{\mu}_{0g}^{(n)}$; $\boldsymbol{\mu}_{0g}^{(n)}$ signifies a $0 \rightarrow g$ transition moment at an nth position $\boldsymbol{R}_n^g$.

After all, a newly extended Fano-DeVoe model Hamiltonian may be assumed as

$$\begin{aligned} H &= \sum_{m=1}^{N}\sum_{f\neq 0}\hbar\omega_{f0}^{(m)}|fm><fm| \\ &\quad + \left\{\sum_{m=1}^{N}\sum_{f\neq 0}|fm>V_{mm}^{ff}<fm| \right. \\ &\quad + \left(\sum_{m=1}^{N}\sum_{f>g;\, f\neq 0,}\sum_{g\neq 0}|fm>V_{mm}^{fg}<gm| + h.c.\right) \\ &\quad \left. + \left(\sum_{m=1}^{N}\sum_{f\neq 0}\sum_{n>m}^{N}\sum_{g\neq 0}|fm>V_{mm}^{fg}<gn| + h.c.\right)\right\} \\ &\equiv H_0 + V. \end{aligned} \quad (7)$$

2. Polymer Polarizability Tensors in the Newly Extended Fano–DeVoe Model. From Eq. 7, the m, f, n, g-matrix elements of the polymer Green's operator ${}^{\mathrm{p}}G(\omega) = 1/[\hbar\omega - H + i\eta]$ are computed by

$${}^{\mathrm{p}}G_{mn}^{fg}(\omega) \equiv <fm|{}^{\mathrm{p}}G(\omega)|gn> = \{[\mathbf{1} - \boldsymbol{G}(\omega)\boldsymbol{V}]^{-1}\boldsymbol{G}(\omega)\}_{mn}^{fg}. \quad (8)$$

The n, g, n, g-matrix elements of the crude Green's operator $G(\omega) = 1/[\hbar\omega - H_0 + i\eta]$ are defined by

$$G_{nn}^{gg}(\omega) \equiv <gn|G(\omega)|gn> = \frac{1}{\hbar(\omega - \omega_{g0}^{(n)} + i\eta_g^{(n)})}, \quad (9)$$

from which the partial *monomer* polarizability tensor $\boldsymbol{\alpha}_{nn}^{gg}(\omega)$ is given by $-\boldsymbol{\mu}_{0g}^{(n)}G_{nn}^{gg}(\omega)\boldsymbol{\mu}_{g0}^{(n)}$. Thus, the partial *polymer* polarizability tensor ${}^{\mathrm{p}}\boldsymbol{\alpha}_{mn}^{fg}(\omega)$ can be computed by $-\boldsymbol{\mu}_{0f}^{(m)}{}^{\mathrm{p}}G_{mn}^{fg}(\omega)\boldsymbol{\mu}_{g0}^{(n)}$. Until a later section, we assume that η and $\eta_g^{(n)}$ are positive infinitesimals, which ensure that $G(\omega)$ and ${}^{\mathrm{p}}G(\omega)$ are retarded Green's operators.

To see qualitatively how the new diagonal *CAE* energies V_{mm}^{ff} are reflected in the UV and CD profiles, let us assume a special case when these *CAE* energies V_{mm}^{ff} are inappropriately overestimated to be able to neglect other types of inter(sub)-molecular interactions. Namely, let us assume that the elements $<fm|V|sk>$ of V in Eq. 7 are just limited to be diagonal, i.e., $V_{mk}^{fs} = V_{mm}^{ff}\delta_{mk}\delta_{fs}$. Then, from Eq. 8, we have approximately the partial polymer polarizability tensor $-\boldsymbol{\mu}_{0f}^{(m)}{}^{\mathrm{p}}G_{mm}^{ff}(\omega)\boldsymbol{\mu}_{f0}^{(m)}$:

$$
\begin{aligned}
{}^{p}\boldsymbol{\alpha}_{mm}^{ff}(\omega) &= -\boldsymbol{\mu}_{0f}^{(m)}\frac{1}{[G_{mm}^{ff}(\omega)]^{-1} - V_{mm}^{ff}}\boldsymbol{\mu}_{f0}^{(m)} \\
&= \frac{-\boldsymbol{\mu}_{0f}^{(m)}\boldsymbol{\mu}_{f0}^{(m)}}{\hbar\omega - \hbar\omega_{f0}^{(m)} - V_{mm}^{ff} + i\eta_f^{(m)}},
\end{aligned} \tag{10}
$$

which explains qualitatively the spectral shift by V_{mm}^{ff} from $\hbar\omega_{f0}^{(m)}$. Here, as the general case, we exactly solve the inverse matrix of the polymer Green's matrix equation given in the braces of Eq. 8. In this way, the new matrix elements V_{mm}^{ff} bring about appropriate spectral shifts in the CD and UV bands; the comparison of the numerical results will be made in Figs. 3 and 4 in the last section.

3. Chiral Polarizability Tensors for a Polymer and Monomers. 3-A. Monomer Chiral Polarizability Tensor: Quantum-mechanically, Eyring et al.[17] presents the derivation of the scalar chiral polarizability $\beta(\nu)$ for a free molecule

$$
\begin{aligned}
\beta(\omega) &= \frac{2c}{3\hbar}\sum_{g\neq 0}^{levels}\frac{\mathrm{Im}[\boldsymbol{\mu}_{0g}\cdot\boldsymbol{m}_{g0}]}{\omega_{g0}^2 - \omega^2 - i2\omega\eta_g} \\
&= \frac{1}{3}\mathrm{Tr}\left[\frac{2c}{\hbar}\sum_{g\neq 0}^{levels}\frac{\mathrm{Im}[\boldsymbol{\mu}_{0g}\boldsymbol{m}_{g0}]}{\omega_{g0}^2 - \omega^2 - i2\omega\eta_g}\right] \equiv \frac{1}{3}\mathrm{Tr}\boldsymbol{\beta}(\omega),
\end{aligned} \tag{11}
$$

where $\eta_g = 0$ and $\mathrm{Tr}\,[\boldsymbol{\mu}_{0g}\boldsymbol{m}_{g0}] = \boldsymbol{\mu}_{0g}\cdot\boldsymbol{m}_{g0}$. Again, η_g introduced above is assumed to be infinitesimal until the later section. Pertaining to Eq. 11, we make use of the following relationships:

$$
\begin{aligned}
&\frac{1}{\omega_{g0}^2 - \omega^2 - i2\omega\eta_g} \\
&= \frac{1}{2\omega_{g0}}\left(\frac{-1}{\omega - \omega_{g0} + i\eta_g} + \frac{1}{\omega + \omega_{g0} + i\eta_g}\right) \\
&= \frac{1}{2\omega + i2\eta_g}\left(\frac{-1}{\omega - \omega_{g0} + i\eta_g} + \frac{-1}{\omega + \omega_{g0} + i\eta_g}\right) \\
&\approx \frac{-1}{2\omega[\omega - \omega_{g0} + i\eta_g]}
\end{aligned} \tag{12}
$$

where neglecting each term involving $(\omega + \omega_{g0} + i\eta_g)$, one can assume $\omega_{g0} \approx \omega$ in the gth transition region of interest. In the CD and UV band shape calculations, it was numerically checked that the approximation of Eq. 12 is correct even for finite values of η_g. Then, the chiral polarizability tensor of the free molecule can immediately be defined in terms of Green's operator $G(\omega) = 1/[\hbar\omega - H_{\mathrm{free}} + i\eta]$ as follows:

$$
\begin{aligned}
\boldsymbol{\beta}(\omega) &\approx -c\sum_{g\neq 0}\boldsymbol{\mu}_{0g}\frac{<g|G(\omega)|g>}{\omega}\mathrm{Im}\,\boldsymbol{m}_{g0} \\
&= -c<0|\boldsymbol{\mu}\frac{G(\omega)}{\omega}\mathrm{Im}\,\boldsymbol{m}|0>,
\end{aligned} \tag{13}
$$

with

$$
H_{\mathrm{free}}|g> = \hbar\omega_{g0}|g>, \tag{14}
$$

where gth state functions $|g>$ is assumed to satisfy the closure relation $\Sigma_g\,|g><g| = 1$. Here, $\boldsymbol{\mu}$ and $\boldsymbol{m}$ are respectively the electric and magnetic dipole moment operators of the free molecule, so that $\boldsymbol{\beta}(\omega)$ is defined in terms of $G^{gg}(\omega) = 1/\hbar\,(\omega - \omega_{g0} + i\eta_g)$. To specify an nth monomer in a certain polymer for $\boldsymbol{\beta}(\omega)$, the nth (*full*) monomer chiral polarizability tensor is written as follows:

$$
\boldsymbol{\beta}_{nn}(\omega) \approx -c\sum_{g\neq 0}\boldsymbol{\mu}_{0g}^{(n)}\frac{G_{nn}^{gg}(\omega)}{\omega}\mathrm{Im}\,\boldsymbol{m}_{0g}^{(n)} \equiv \sum_{g\neq 0}\boldsymbol{\beta}_{nn}^{gg}(\omega), \tag{15}
$$

where $\boldsymbol{\beta}_{nn}^{gg}(\omega)$ defines the nth *partial* monomer chiral polarizability tensor for the gth level, Similarly, $\boldsymbol{\alpha}_{nn}^{gg}(\omega)$ mentioned in section 2 is obtained starting from $\alpha(\omega)$ in Ref. 17.

3-B. Polymer Chiral Polarizability Tensor: We define the dipole moment operator for the polymer (N-mer) system:

$$
\boldsymbol{\mu} = \sum_{n=1}^{N}\sum_{i} - e(\boldsymbol{r}_i - \boldsymbol{R}_n) \equiv \sum_{n=1}^{N}\boldsymbol{\mu}^{(n)}, \tag{16}
$$

where $\boldsymbol{\mu}^{(n)}$ denotes the dipole moment operator for the position vector $\boldsymbol{R}_n$ of an nth monomer. Also, the nth monomer magnetic moment operator $\boldsymbol{M}_n$ is defined by

$$
\begin{aligned}
\boldsymbol{M}_n &= \left(\frac{-e}{2mc}\right)\sum_i \boldsymbol{r}_i \times \boldsymbol{p}_i^{(n)} \\
&= \left(\frac{-e}{2mc}\right)\sum_i (\boldsymbol{r}_i - \boldsymbol{R}_n) \times \boldsymbol{p}_i^{(n)} \\
&\quad + \left(\frac{-e}{2mc}\right)\sum_i \boldsymbol{R}_n \times \boldsymbol{p}_i^{(n)},
\end{aligned} \tag{17}
$$

in which the first term denotes the nth local monomer magnetic moment:

$$
\boldsymbol{m}^{(n)} = \left(\frac{-e}{2mc}\right)\sum_i^{electrons}(\boldsymbol{r}_i - \boldsymbol{R}_n) \times \boldsymbol{p}_i^{(n)}, \tag{18}
$$

The total magnetic moment is then given by

$$
\boldsymbol{M} = \sum_{n=1}^{N}\boldsymbol{M}_n = \sum_{n=1}^{N}\boldsymbol{m}^{(n)} + \left(\frac{-e}{2mc}\right)\sum_{n=1}^{N}\sum_i \boldsymbol{R}_n \times \boldsymbol{p}_i^{(n)}. \tag{19}
$$

By making use of the velocity-dipole relation[23] for the λth excited states for a polymer:

$$
\boldsymbol{p}_{\lambda 0}^{(n)} = -\boldsymbol{p}_{0\lambda}^{(n)} = -im\frac{\omega_{\lambda 0}^{(n)}}{e}\boldsymbol{\mu}_{\lambda 0}^{(n)}, \tag{20}
$$

we obtain the total rotatory strength:

$$
\begin{aligned}
&\sum_{\lambda\neq 0}\mathrm{Im}[<0|\boldsymbol{\mu}|\lambda>\cdot<\lambda|\boldsymbol{M}|0>] \\
&= \sum_{\lambda\neq 0}\sum_{m=1}^{N}\sum_{n=1}^{N}\mathrm{Im}\Big\{<0|\boldsymbol{\mu}^{(m)}|\lambda>\cdot<\lambda|\boldsymbol{m}^{(n)}|0> \\
&\quad + \frac{i\omega_{\lambda 0}}{2c}<0|\boldsymbol{\mu}^{(m)}|\lambda>\cdot\boldsymbol{R}_n \times <\lambda|\boldsymbol{\mu}^{(n)}|0>\Big\} \\
&= \sum_{\lambda\neq 0}\sum_{m=1}^{N}\sum_{n=1}^{N}\mathrm{Im}\Big\{<0|\boldsymbol{\mu}^{(m)}|\lambda>\cdot<\lambda|\boldsymbol{m}^{(n)}|0> \\
&\quad + \frac{i\omega_{\lambda 0}}{4c}\boldsymbol{R}_{mn}\cdot<0|\boldsymbol{\mu}^{(n)}|\lambda> \times <\lambda|\boldsymbol{\mu}^{(m)}|0>\Big\},
\end{aligned} \tag{21a}
$$

$$= \sum_{\lambda\neq 0}\sum_{m=1}^{N}\sum_{n=1}^{N}\Big\{\mathrm{Tr\ Im}[<0|\boldsymbol{\mu}^{(m)}|\lambda><\lambda|\boldsymbol{m}^{(n)}|0>] + \frac{i\omega_{\lambda 0}}{4c}\boldsymbol{R}_{mn}\cdot[<0|\boldsymbol{\mu}^{(m)}|\lambda><\lambda|\boldsymbol{\mu}^{(n)}|0>:\boldsymbol{\varepsilon}]\Big\}, \quad (21b)$$

where it is assumed that $\Sigma_\lambda|\lambda><\lambda| = 1$ holds for λth state functions of the polymer Hamiltonian. In Eq. 21b, $\boldsymbol{\varepsilon}$ signifies the Levi–Civita tensor,[24] the second term corresponds to the $\boldsymbol{\mu}$–$\boldsymbol{\mu}$ interaction mechanism derived by Condon,[25] and the first term represents the $\boldsymbol{\mu}$–$\boldsymbol{m}$ mechanisms.[26]

From Eq. 11 using Eqs. 12 and 21b, we can define the polymer scalar chiral polarizability:

$$\begin{aligned}{}^{polymer}\beta(\omega) &= \frac{c}{3\hbar}\sum_{\lambda\neq 0}\frac{\mathrm{Im}[<0|\boldsymbol{\mu}|\lambda>\cdot<\lambda|\boldsymbol{M}|0>]}{\omega_{\lambda 0}^2 - \omega^2 - i2\omega\eta_\lambda}\\ &\approx -\frac{c}{3}\mathrm{Tr}<0|\boldsymbol{\mu}\frac{{}^pG(\omega)}{\omega}\mathrm{Im}\,\boldsymbol{m}|0>\\ &\quad -\frac{1}{12}\sum_{m=1}^{N}\sum_{n=1}^{N}\boldsymbol{R}_{mn}\cdot<0|\boldsymbol{\mu}^{(m)}\,{}^pG(\omega)\boldsymbol{\mu}^{(n)}|0>:\boldsymbol{\varepsilon}\\ &\equiv {}^p\beta_{\mu-m}(\omega) + {}^p\beta_{\mu-\mu}(\omega). \end{aligned} \quad (22)$$

Inserting the resolution of identity into the second term ${}^p\beta_{\mu-\mu}(\omega)$ of Eq. 22, we obtain the $\boldsymbol{\mu}$–$\boldsymbol{\mu}$ part of the scalar polymer chiral polarizability:

$${}^p\beta_{\mu-\mu}(\omega) = -\frac{1}{12}\sum_{m=1}^{N}\sum_{n=1}^{N}\sum_{f\neq 0}\sum_{g\neq 0}\boldsymbol{R}_{mn}\cdot\boldsymbol{\mu}_{0f}^{(m)}\,{}^pG_{mn}^{fg}(\omega)\boldsymbol{\mu}_{g0}^{(n)}:\boldsymbol{\varepsilon}, \quad (23a)$$

which was classically derived by Buckingham and Stiles,[15] DeVoe,[21,22] and Applequist.[24] In Eqs. 21, 22, and 23a, a distance vector $\boldsymbol{R}_{mn}$ comes from the position operator $\boldsymbol{R}_n$ of Eq. 19. Clearly, $\boldsymbol{R}_m$ and $\boldsymbol{R}_n$ are associated with the transition dipole centers $\boldsymbol{R}_m^f$ and $\boldsymbol{R}_n^g$ for $\boldsymbol{\mu}_{0f}^{(m)}$ and $\boldsymbol{\mu}_{g0}^{(n)}$ through Eqs. 20 and 21. Namely, we represent $\boldsymbol{R}_n$ by $\boldsymbol{R}_n{}^g$ explicitly to show the gth level-dependence. Therefore, for a distance vector $\boldsymbol{R}_{mn}^{fg}$ ($\equiv \boldsymbol{R}_n^g - \boldsymbol{R}_m^f$), the scalar polymer chiral polarizabity may be in general given by

$${}^p\beta_{\mu-\mu}(\omega) = -\frac{1}{12}\sum_{m=1}^{N}\sum_{n=1}^{N}\sum_{f\neq 0}\sum_{g\neq 0}\boldsymbol{R}_{mn}^{fg}\cdot\boldsymbol{\mu}_{0f}^{(m)}\,{}^pG_{mn}^{fg}(\omega)\boldsymbol{\mu}_{g0}^{(n)}:\boldsymbol{\varepsilon}, \quad (23b)$$

We can derive Eq. 23b from the beginning rather than intuitively assuming Eq. 23b from Eq. 23a, if we consider the double appearances of ($\boldsymbol{R}_m^f$, $\boldsymbol{R}_n^g$) and ($\boldsymbol{R}_n^g$, $\boldsymbol{R}_m^f$) in the following sum:

$$\begin{aligned}{}^p\beta(\omega) &\approx -\frac{c}{3\hbar}<0|\boldsymbol{\mu}\frac{{}^pG(\omega)}{\omega}\cdot\mathrm{Im}\,\boldsymbol{M}|0> = \frac{1}{3}\mathrm{Tr}\,{}^p\boldsymbol{\beta}(\omega)\\ &= \sum_{m=1}^{N}\sum_{f\neq 0}\sum_{n=1}^{N}\sum_{g\neq 0}\Big\{-\frac{c}{3}\boldsymbol{\mu}_{0f}^{(m)}\,{}^pG_{mn}^{fg}(\omega)\cdot\mathrm{Im}\,\boldsymbol{m}_{g0}^{(n)}/\omega\\ &\quad -\frac{1}{6}\omega_{g0}^{(n)}\boldsymbol{\mu}_{0f}^{(m)}\,{}^pG_{mn}^{fg}(\omega)\cdot\boldsymbol{R}_n^g\times\boldsymbol{\mu}_{g0}^{(n)}/\omega\Big\}\\ &\equiv {}^p\boldsymbol{\beta}_{\mu-m}(\omega) + {}^p\beta_{\mu-\mu}(\omega). \end{aligned} \quad (24)$$

After all, the last term of Eq. 24 becomes Eq. 23b, if we consider that we can assume $\omega_{g0}^{(n)} \approx \omega$ in the related spectral regions.

3-C. CD and UV Band Shape Funtions: In pevious sections, η and η_g are assumed to be infinitesimals. This means that in the numerical calculations, η and η_g appearing in the denominators of polarizabilities must be chosen to be sufficiently small so that the limits of η and η_g are meaningfully computed, but η and η_g must be large enough to reproduce the experimentally observed UV and CD curves. Since the chiral polarizability of Eyring et al. is just for $\eta_g = 0$ in Eq. 11, $\beta(\omega)$ diverges at the resonance energy $\hbar\omega_{g0}^{(n)}$, so that their $\beta(\omega)$ applies only outside of resonance regions. However, at the resonance points for the chiral and electric polarizabilities $\beta(\omega)$ and $\alpha(\omega)$, many investigators make use of finite but sufficiently small values for η and η_g; the often used damping factor $\eta_g^{(n)} = \Gamma_g^{(n)}/2$ is taken to be the half-width at half-height (HWHH) of the experimentally observed gth Lorentzian band, $\Gamma_g^{(n)}$ being the full-width. Even in this compromised choice of η_g, the relationships $\omega_{g0}^{(n)} \gg \eta_g$ must be presumed. Then, we must consider what the finite value of η_g means. The damped oscillator model may be an answer to this.[30,31] Another answer may follow from the Fourier transform of $\alpha_{mn}^{gg}(\omega)$ which leads to $\alpha_{mn}^{gg}(t) = |\boldsymbol{\mu}_{0g}|^2/\hbar\, exp(-i\omega_{g0}^{(n)}t)exp(-\eta_g t)$.[32] This shows that the dipole strength $|\boldsymbol{\mu}_{0g}|^2$ with finite lifetime $1/\eta_g$ decays according to $exp(-\eta_g t)$.

The CD band shape function is given in units of deg cm^2 dmol^{-1} by:[1]

$$[\theta(\omega)] = \frac{72N_A}{c^2}\omega^2\frac{1}{N}\sum_{m=1}^{N}\sum_{n=1}^{N}\sum_{f\neq 0}^{levels}\sum_{g\neq 0}^{levels}\mathrm{Im}\{-\frac{1}{12}\boldsymbol{R}_{mn}^{fg}\cdot\boldsymbol{\mu}_{0f}^{(m)}\,{}^pG_{mn}^{fg}(\omega)\boldsymbol{\mu}_{g0}^{(n)}:\boldsymbol{\varepsilon} - \frac{1}{3}\mathrm{Tr}[\frac{1}{2\pi}\boldsymbol{\mu}_{0f}^{(m)}\frac{{}^pG_{mn}^{fg}(\omega)}{\omega}\mathrm{Im}\,\boldsymbol{m}_{g0}^{(n)}]\}. \quad (25)$$

The UV/vis absorption band shape function is computed in units of dm^3 mol^{-1} cm^{-1} by:

$${}^p\varepsilon(\omega) = \frac{4\pi N_A}{2302.6c}\omega\frac{1}{N}\sum_{m=1}^{N}\sum_{n=1}^{N}\mathrm{Im}[\frac{1}{3}\mathrm{Tr}\sum_{f\neq 0}^{levels}\sum_{g\neq 0}^{levels}{}^p\boldsymbol{\alpha}_{mn}^{fg}(\omega)]. \quad (26)$$

4. Lorentzian and Gaussian Approximations for the Imaginary Part of an *n*th Monomer Polarizability Tensor. In the classical forced oscillator models and the quantum theories,[30,31] the absorption curve is shown to exhibit the Lorentzian behavior associated with natural line widths. Guassian profiles are produced by the random thermal motion; the Gaussian behavior is understood by the Doppler effect calculated from the Boltzmann distribution of the velocities of the oscillators and atom[31] or molecules.[33] In general, however, it appears theoretically difficult to make simple predictions for the monomer band shapes for complex molecules. In the actual CD and UV calculations of polymer systems based upon monomer absorption and dispersion curves, the Lorentzian and Gaussian shapes are emprically and widely used ;[27,29,34] the absorption UV curves are related to Im $\alpha_{nn}^{gg}(\omega)$ with the finite HWHH $\eta_{g,L}^{(n)}$ and $\eta_{g,G}^{(n)}$. In the symbolic identity:

$$\frac{1}{E - E_{g0}^{(n)} + i\eta_{g,L\,\mathrm{or}\,G}^{(n)}} = \mathcal{P}\frac{1}{E - E_{g0}^{(n)}} - i\pi\delta(E - E_{g0}^{(n)}), \quad (27)$$

where $\eta_{g,L}^{(n)}$ and $\eta_{g,G}^{(n)}$ are sufficiently small, we can relate the Dirac delta function with the two types of delta function forms well-known for the Gaussian function and the Lorentzian function.[35] For the Dirac delta function, Briggs and Herzenberg have employed a Gaussian curve having the finite η_g for the UV band of J-aggregates,[36] simply regarding a single UV band

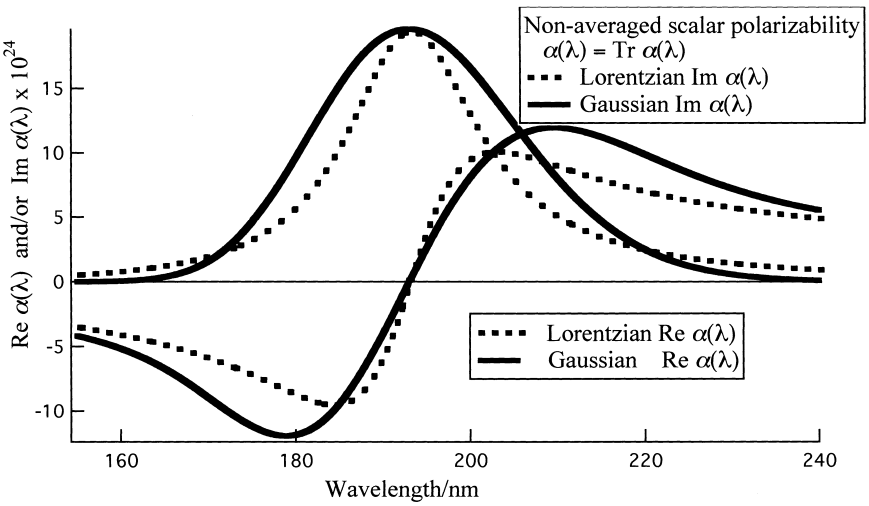

Fig. 1. Wavelength dependence of the real and imaginary parts of the Gaussian and Lorentzian types of non-averaged scalar polarizabilities for the 193 nm $\pi\pi^*$ band ($= \lambda_{g0}^{(n)}$) of an amide molecule with $\eta_{g,L}^{(n)} = 1500$ cm^{-1}, $\Delta_g^{(n)} = \sqrt{\pi}\ \eta_{g,L}^{(n)}$, and the oscillator strength $f_g^{(n)} = 0.237$.

as a vibrational envelope. By the reasonings given in section **3-C**, we also use the finite η_L and η_G for infinitesimally small quantities assumed in the previous sections.

Then, the imaginary part for the Lorentzian type of polarizability is obtained by:

$$\alpha_{nn}^{gg}(\omega) = \frac{1}{3}\mathrm{Tr}\boldsymbol{\alpha}_{nn}^{gg}(\omega) = \frac{-\boldsymbol{\mu}_{0g}^{(n)}\cdot\boldsymbol{\mu}_{g0}^{(n)}}{3\hbar[\omega - \omega_{g0}^{(n)} + i\eta_g^{(n)}]} = \left(\frac{-\boldsymbol{\mu}_{0g}^{(n)}\cdot\boldsymbol{\mu}_{g0}^{(n)}}{3\hbar}\right)\frac{(\omega - \omega_{g0}^{(n)}) - i\eta_g^{(n)}}{(\omega - \omega_{g0}^{(n)})^2 + (\eta_g^{(n)})^2}. \quad (28)$$

The imaginary part for the Gaussian type of polarizability is given by:

$$\mathrm{Im}\,\alpha_{nn}^{gg}(\omega) = \frac{1}{3\hbar}\boldsymbol{\mu}_{0g}^{(n)}\cdot\boldsymbol{\mu}_{g0}^{(n)}\frac{\sqrt{\pi}}{\Delta_g^{(n)}}\exp\left[-\left(\frac{\omega - \omega_{0g}^{(n)}}{\Delta_g^{(n)}}\right)^2\right], \quad (29)$$

where $\Delta g^{(n)}$ is the half-width at the $1/e$ of the peak height for the Gaussian band; for the half-width $\eta_g^{(n)}$ and the full-width $\Gamma_g^{(n)}$, we have the relationship[27] $\Gamma_g^{(n)} = 2\sqrt{ln2}\Delta_g^{(n)} = 2\eta_g^{(n)}$. To choose a reasonable Gaussian half-width $\Delta_g^{(n)}$, one can also derive such a useful relationship as $\Delta_g^{(n)} = \sqrt{\pi}\,\eta_{g,L}^{(n)}$. To derive Re $\alpha_{nn}^{gg}(\omega)$, we make use of the Kramers-Kronig relation:

$$\mathrm{Re}\,\alpha_{nn}^{gg}(\omega) = \frac{\mathcal{P}}{\pi}\int_{-\infty}^{\infty}\frac{\mathrm{Im}\alpha_{nn}^{gg}(\omega')}{\omega' - \omega}d\omega' = \left(\frac{\sqrt{\pi}|\boldsymbol{\mu}_{0g}^{(n)}|^2}{3\hbar\Delta_g^{(n)}}\right)\frac{\mathcal{P}}{\pi}\int_{-\infty}^{\infty}\frac{\exp\{-\omega''^2\}}{\omega'' - (\omega - \omega_{g0}^{(n)})/\Delta_g^{(n)}}d\omega''. \quad (30)$$

We must then determine the integral of the form of

$$f(z) = \mathcal{P}\int\exp(-x'^2)/(x' - z)dx',$$

which can be derived in a way similar to that by which Wyld derived the same kind of integral.[28] Starting with z in the upper half of the z-plane, but moving z up onto the real axis, we obtain a Dawson integral:[29]

$$\mathcal{P}\int_{-\infty}^{\infty}\frac{\exp(-z^2)}{z \pm a}dz = \pm 2\sqrt{\pi}\exp(-a^2)\int_0^a\exp(+z^2)dz. \quad (31)$$

From Eq. 31, we thus obtain

$$\mathrm{Re}\,\alpha_{nn}^{gg}(\omega) = \frac{|\boldsymbol{\mu}_{g0}^{(n)}|^2}{3\hbar}\frac{1}{\sqrt{\pi}\Delta_g^{(n)}} \times 2\sqrt{\pi}\exp\left[-\left(\frac{\omega - \omega_{g0}^{(n)}}{\Delta_g^{(n)}}\right)^2\right]\int_0^{(\omega_{g0}^{(n)} - \omega)/\Delta_g^{(n)}}\exp(+y^2)dy. \quad (32)$$

For $\pm(\omega - \omega_{g0}^{(n)}) > 0$, from Eq. 31, we can have

$$\mathrm{Re}\,\alpha_{nn}^{gg}(\omega) = \mp\frac{2|\boldsymbol{\mu}_{g0}^{(n)}|^2}{3\hbar\Delta_g^{(n)}}\exp\left[-\left(\frac{\omega - \omega_{g0}^{(n)}}{\Delta_g^{(n)}}\right)^2\right]\int_0^{|(\omega - \omega_{g0}^{(n)})/\Delta_g^{(n)}|}\exp(+y^2)dy. \quad (33)$$

As shown in Fig. 1, whose conceptual features are separately shown in various textbooks[29,30] except for that of a Gaussian dispersion curve, Eq. 33 gives rise to the Gaussian dispersion curve which is rather different from the Lorentzian dispersion curve. We can numerically compute the Dawson integral[29,34,36,37] using Simpsons' formula and/or Newton–Cotes' formula.[37]

Results and Discussion

To compute Eqs. 25 and 26, one can approximate monomer electric and chiral polarizabilties together with Eq. 9 using the monomer spectroscopic parameters of formamide $HCONH_2$ (C_{1h} symmetry) and the three typically assumed conformers *N*, *P*, and *PN* (C_{1h}) of myristamide $CH_3(CH_2)_{12}CONH_2$; conformer *PN* is shown in Fig. 2.

1. Computed Results of Monomer Spectroscopic Properties. From large CI calculations by the CNDO/S method,[8–10] we took into account only the two low-lying $n\pi^*$ and $\pi\pi^*$ transition states for the monomer amides. In Tables 1, 2, and 3, we

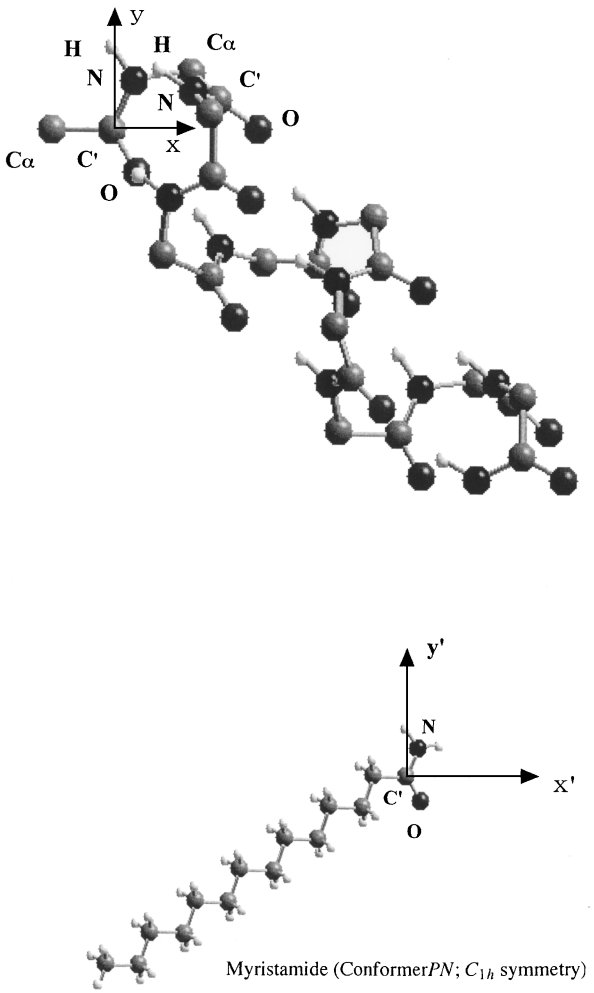

Fig. 2. First amide chromophore ($n = 1$) of a polypeptide on which the Cartesian coordinate system is assumed. Formamide and the three kinds of conformers (*N*, *PN*, and *P*) of myristamide are superposed on this *x*, *y*-coordinates;[1] when polymers are constituted from the conformers of myristamide chromophores, the bulky size of tridecyl group is ignored. The $C_{\alpha,n-1}(C'ONH)_n$-units are taken in the same plane. Regarding myristamide, we assume $\boldsymbol{R}_{C'\text{-}C} = \boldsymbol{R}_{C\text{-}C} = 1.53$ Å, $\boldsymbol{R}_{C\text{-}H} = 1.00$ Å, and $\boldsymbol{R}_{N\text{-}H} = 1.00$ Å. For the nearest methylene group to the *x*,*y*-plane of amide as well as for other methylene groups and methyl group, we assume the terahedral angle. For the myristamide with C_{1h} symmetry (conformer *PN*), the nearest H_2C_α—CH_2 bond of the tridecyl group is taken to be eclipsed with the C′O bond of the —C′ONH_2 plane, while for an optical active conformer *P* and/or *N*, the one of two $C_\alpha H$ bonds is assumed to be eclipsed with the C′N bond of the —C′ONH_2 plane. Therefore, the tridecyl group of confomer *P* is in the upper side of the —C′ONH_2 plane, while that of the conformer *N* is in the lower side of the —C′ONH_2 plane.

listed the necessary monomer spectroscopic properties. The excitation energies in the footnotes were chosen from the empirical values.[1,38–41] Except for these excitation energies and the assumed $\eta_g^{(n)}$, we used the values computed. The dipole positions for $\boldsymbol{\mu}_{0f}^{(m)}$, $\boldsymbol{\mu}_{fg}^{(m)}$, $\boldsymbol{\mu}_{ff}^{(m)}$, and $\boldsymbol{\mu}_{00}^{(m)}$ were put on the centers of gravity simply for *four* limited absolute atomic transition charges in —$(C'ONH)_m$—.

Also, in Tables 1, 2, and 3, the $n\pi^*$ magnetic moment directions and the $\pi\pi^*$ electric transition moment directions are given. As shown in Tables 2 and 3, the projected angle $\angle\mu_{\pi\pi^*}$–$\overline{C'O}$ between the $\pi\pi^*$ electric transition moment and the carbonyl bond for the conformers of myristamide agree poorly with the experimental value of $-35° \pm 3°$.[42,43] As far as the directions of transition moments are concerned, the achiral formamide seems to be preferable as an amide chromophore available to the chiral and achiral myristamide conformers. However, the oscillator strength of the $\pi\pi^*$ transition is underestimated by a factor of 2.53, which means that the $\pi\pi^*$ transition moment is underestimated by a factor of 1.59 ($= \sqrt{2.53}$). Also, the calculated oscillator strengths of the $\pi\pi^*$ transitions of the three conformers assumed for myristamide are underestimated by factors 1.37 and 1.32.

In addition to the above-mentioned large deviations from observed transition directions,[42,43] Clark showed that the $\pi\pi^*$ transition moment is polarized at $-55° \pm 5°$ for *N*-acetylglycine which is a model compound of secondary amides;[42] the secondary amides are in general constituent chromophores in polypeptides. His observation indicates that neither the chiral conformers *N* and *P* nor the achiral conformer *PN* of myristamide are good model chromophores for polypeptides. In spite of this discrepancy, to see how the present theory works, we carried out the CD calculations using the monomer properties of chiral and achiral myristamides as well as formamide.

The monomer properties of Tables 1 and 2 assume the use of intrinsically optical inactive monomers (C_{1h}) for polypeptides, whereas those of Table 3 assume the use of intrinsically optical active monomers. A similar example for the former case may be the CD study of cyclic amide dimers presented by Bowman et al.[40] For the latter case, the formulations[1,14–16,20] involving the chiral polarizabilities may be convenient. Keeping in mind appropriate chiral chromophores in polypeptides, Volosov carried out the calculation of rotational strengths for myristamide;[44] his CNDO/OPTIC results for the crystal structure, i.e., $\boldsymbol{R}_{n\pi^*}^{(n)} = +0.08843$ DBM ($+ 8.2 \times 10^{-40}$ cgs) and $\boldsymbol{R}_{\pi\pi^*}^{(n)} = -0.00647$ DBM (-0.6×10^{-40} cgs) can be compared with the results of Table 3 ($\boldsymbol{R}_{n\pi^*}^{(n)} = \mp 0.01442$ DBM and $\boldsymbol{R}_{\pi\pi^*}^{(n)} = \mp 0.03754$ DBM for conformers *N* and *P*). The upper negative sign is associated with the conformer *N*; several investigators[40,45–47] have also shown that the amide chromophores having the negative $n\pi^*$ chiral optical activity could be used as starting monomers.

However, most CD calculations have successfully been carried out based upon achiral amide chromophores, which means that the principal sources of monomer chirality are dissymetric torsion about peptide bonds and pyramidalization at the amide nitrogen.[40,48] Even if this is true, it may be valuable to carry out the CD calculations by employing not only such chiral amide chromophores but also achiral amide chromophores often used as starting monomers. Whichever one may choose, our formulations[1,16,20] may be useful.

2. Computed Results of CD and UV Absorption Curves. The validity of the present method must be examined for the following typical conformations of polypeptides, since changes of the peptide backbone geometry as well as the choice of the monomer spectroscopic paremeters mentioned are sensi-

Table 1. Spectroscopic Monomer Properties Computed by the CNDO/2S Method, for the Two Low-Lying Levels ($n\pi^*$, $\pi\pi^*$) of All the Possible 54 × 54 Singly-Excited Configuration Interaction Calculations of the Achiral *Formamide* Chromophore (C_{1h} symmetry)

gth State	$\hbar\omega_{g0}^{(n)}$	$(\lambda_{g0}^{(n)})$	$f_{0g}^{(n)}$	[Exptl.; $\hbar\omega_{g0}^{(n)}$ $(\lambda_{g0}^{(n)})$, $f_{0g}^{(n)}$]
$n\pi^*$	4.74 eV	(262 nm)	0.00854	[5.65 eV (219 nm), 0.002][a]
$\pi\pi^*$	7.76 eV	(160 nm)	0.09504	[7.32 eV (169 nm), 0.240]
$\boldsymbol{\mu}_{n\pi^*}^{(n)}/e$	(0.00000, 0.00000, 0.14356 Å)[b]			out-of-plane
$\boldsymbol{m}_{n\pi^*}^{(n)}$	(−0.42567, 0.73605, 0.00000 BM)			in-plane ($\angle \boldsymbol{m}_{n\pi^*}$–X-axis = 59.9°)[d]
$\boldsymbol{\mu}_{\pi\pi^*}^{(n)}/e$	(0.01407, 0.37379, 0.00000 Å)[b]			in-plane ($\angle \boldsymbol{\mu}_{\pi\pi^*}$–$\overline{\mathrm{C'O}}$ = −33.2°)[d]
$\boldsymbol{m}_{\pi\pi^*}^{(n)}$	(0.00000, 0.00000, 0.55834 BM)			out-of-plane
$\boldsymbol{\mu}_{n\pi^*,\pi\pi^*}^{(n)}/e = \boldsymbol{\mu}_{\pi\pi^*,n\pi^*}^{(n)}/e$	(0.00000, 0.00000, 0.16065 Å)[b]			out-of-plane
$\boldsymbol{\mu}_{n\pi^*,n\pi^*}^{(n)}/e$	(−0.13414, 0.38017, 0.00000 Å)[c]			in-plane
$\boldsymbol{\mu}_{\pi\pi^*,\pi\pi^*}^{(n)}/e$	(−0.00893, 1.31831, 0.00000 Å)[c]			in-plane
$\boldsymbol{\mu}_{00}^{(n)}$	(−1.81188, 4.93453, 0.00000 Debye)[c]			in-plane

a) Refs. 41, 42, 43, and 46. Regarding the parameterization, see Ref. 1. For $n\pi^*$ and $\pi\pi^*$ transition energies, we use the experimentally assumed values of $\lambda_{g0}^{(n)}$ = 210 nm and 185 nm with the same damping factor $\eta_g^{(n)}$ = 1500 cm^{-1}. b) By the dipole-velocity method. c) The dipole-length method, by which the following results were obtained;
$\boldsymbol{\mu}_{n\pi^*}^{(n)}/e$ (0.00000, 0.00000, 0.04141 Å), out-of-plane, $f_{n\pi^*}^{(n)}$= 0.00071
$\boldsymbol{\mu}_{\pi\pi^*}^{(n)}/e$ (−0.10533, −0.73058, 0.00000 Å), in-plane ($\angle\mu_{\pi\pi^*}$–$\overline{\mathrm{C'O}}$ = −39.2°), $f_{\pi\pi^*}^{(n)}$= 0.37009
$\boldsymbol{\mu}_{n\pi^*,\pi\pi^*}^{(n)}/e = \boldsymbol{\mu}_{\pi\pi^*,n\pi^*}^{(n)}/e$ (0.00000, 0.00000, 0.05639 Å), out-of-plane.
Note that diagonal types of moments such as $\boldsymbol{\mu}_{00}^{(n)}$, $\boldsymbol{\mu}_{n\pi^*,n\pi^*}^{(n)}$, and $\boldsymbol{\mu}_{\pi\pi^*,\pi\pi^*}^{(n)}$ have no choice except for the dipole-length method. d) An angle measured down from the x-axis of the amide plane; for the $\overline{\mathrm{C'O}}$ reference axis, a positive angle is measured toward the N-atom of the amide; the experimental value of −35° ± 3°, which corresponds to 9.1° toward the C′N bond direction from the NO direction.

Table 2. Spectroscopic Monomer Properties Computed by the CNDO/2S Method, for the Two Low-Lying Levels ($n\pi^*$, $\pi\pi^*$) of the Limited 120 × 120 Singly-Excited CI Calculations (12 occ. MO's → 10 unocc. MO's) of the Achiral *Myristamide* Chromophore (Conformer *PN*, C_{1h})

gth State	$\hbar\omega_{g0}^{(n)}$	$(\lambda_{g0}^{(n)})$	$f_{0g}^{(n)}$	[Exptl.; $\hbar\omega_{g0}^{(n)}$ $(\lambda_{g0}^{(n)})$, $f_{0g}^{(n)}$]
$n\pi^*$	4.82 eV	(257 nm)	0.01029	[5.65 eV (219 nm), 0.002][a]
$\pi\pi^*$	8.26 eV	(150 nm)	0.17516	[7.32 eV (169 nm), 0.240]
$\boldsymbol{\mu}_{n\pi^*}^{(n)}/e$	(0.00000, 0.00000, −0.15614 Å),[b]			out-of-plane
$\boldsymbol{m}_{n\pi^*}^{(n)}$	(0.38788, −0.82976, 0.00000 BM),			in-plane ($\angle \boldsymbol{m}_{n\pi^*}$–X-axis = 64.9°)[d]
$\boldsymbol{\mu}_{\pi\pi^*}^{(n)}/e$	(0.09140, −0.48385, 0.00000 Å),[b]			in-plane ($\angle \mu_{\pi\pi^*}$–$\overline{\mathrm{C'O}}$ = −20.5°)[d]
$\boldsymbol{m}_{\pi\pi^*}^{(n)}$	(0.00000, 0.00000, −0.85312 BM),			out-of-plane
$\boldsymbol{\mu}_{n\pi^*,\pi\pi^*}^{(n)}/e = \boldsymbol{\mu}_{\pi\pi^*,n\pi^*}^{(n)}/e$	(0.00000, 0.00000, 0.12288 Å)[b]			out-of-plane
$\boldsymbol{\mu}_{n\pi^*,n\pi^*}^{(n)}/e$	(−0.35144, 0.41542, 0.00000 Å)[c]			in-plane
$\boldsymbol{\mu}_{\pi\pi^*,\pi\pi^*}^{(n)}/e$	(−0.09566, 1.24925, 0.00000 Å)[c]			in-plane
$\boldsymbol{\mu}_{00}^{(n)}$	(−2.41865, 4.82844, 0.00000 Debye),[c]			in-plane

a) Refs. 41, 42, 43, and 46. Regarding parameterization, see Ref. 1. For $n\pi^*$ and $\pi\pi^*$ transition energies, we use the experimentally assumed values of $\lambda_{g0}^{(n)}$ = 210 nm and 185 nm with the same damping factor $\eta_g^{(n)}$ =1500 cm^{-1}. b) By the dipole-velocity method. c) The dipole-length method, by which the following results were obtained;
$\boldsymbol{\mu}_{n\pi^*}^{(n)}/e$ (0.00000, 0.00000, 0.06507 Å), out-of-plane, $f_{n\pi^*}^{(n)}$= 0.00179
$\boldsymbol{\mu}_{\pi\pi^*}^{(n)}/e$ (0.17281, −0.76240, 0.00000 Å), in-plane ($\angle\boldsymbol{\mu}_{\pi\pi^*}$–$\overline{\mathrm{C'O}}$ = −21.5°), $f_{\pi\pi^*}^{(n)}$= 0.44148
$\boldsymbol{\mu}_{n\pi^*,\pi\pi^*}^{(n)}/e = \boldsymbol{\mu}_{\pi\pi^*,n\pi^*}^{(n)}/e$ (0.00000, 0.00000, 0.06527 Å), out-of-plane.
d) An angle measured down from the x-axis of the amide plane; for the $\overline{\mathrm{C'O}}$ reference axis, a positive angle is measured toward the N-atom of the amide.
Atomic transition charge densities of amide chromophore (—C′ONH—);

$q_{n\pi^*}^{C'}$	= −0.09987	$q_{n\pi^*}^{O}$	= 0.00469	$q_{n\pi^*}^{N}$	= −0.04163	$q_{n\pi^*}^{H}$	= −0.00003
$q_{\pi\pi^*}^{C'}$	= 0.19127	$q_{\pi\pi^*}^{O}$	= −0.44166	$q_{\pi\pi^*}^{N}$	= 0.26955	$q_{\pi\pi^*}^{H}$	= −0.00276
$q_{n\pi^*n\pi^*}^{C'}$	= 0.09310	$q_{n\pi^*n\pi^*}^{O}$	= 0.19945	$q_{n\pi^*n\pi^*}^{N}$	= −0.52065	$q_{n\pi^*n\pi^*}^{H}$	= 0.18028
$q_{\pi\pi^*\pi\pi^*}^{C'}$	= 0.09094	$q_{\pi\pi^*\pi\pi^*}^{O}$	= −0.04125	$q_{\pi\pi^*\pi\pi^*}^{N}$	= −0.03512	$q_{\pi\pi^*\pi\pi^*}^{H}$	= 0.17652
$q_{n\pi^*\pi\pi^*}^{C'}$	= $q_{\pi\pi^*n\pi^*}^{C'}$	$q_{n\pi^*\pi\pi^*}^{O}$	= $q_{\pi\pi^*n\pi^*}^{O}$	$q_{n\pi^*\pi\pi^*}^{N}$	= $q_{\pi\pi^*n\pi^*}^{N}$	$q_{n\pi^*\pi\pi^*}^{H}$	= $q_{\pi\pi^*n\pi^*}^{H}$
	= −0.04684		= −0.01693		= −0.09333		= −0.00007
$q_{00}^{C'}$	= 0.75074	q_{00}^{O}	= −0.30359	q_{00}^{N}	= −0.43993	q_{00}^{H}	= 0.17889

Table 3. Spectroscopic Monomer Properties Computed by the CNDO/2S Method, for the Two Low-Lying Levels ($n\pi^*$, $\pi\pi^*$) of the Limited 120 × 120 Singly-Excited CI Calculations (12 occ. MO's → 10 unocc. MO's) of the Chiral *myristamide* Chromophores (Conformer ($^{N}_{P}$)), where ± and ∓ Values Correspond, Respectively, to Values for Conformer ($^{N}_{P}$)

gth State	$\hbar\omega_{g0}^{(n)}$	$(\lambda_{g0}^{(n)})$	$f_{0g}^{(n)}$	[Exptl.; $\hbar\omega_{g0}^{(n)}$ $(\lambda_{g0}^{(n)})$, $f_{0g}^{(n)}$]
$n\pi^*$	4.83 eV	(257 nm)	0.01079	[5.65 eV (219 nm), 0.002][a]
$\pi\pi^*$	8.25 eV	(150 nm)	0.18117	[7.32 eV (169 nm), 0.240]
$\boldsymbol{\mu}_{n\pi^*}^{(n)}/e$	(−0.00476,	0.00154, ∓0.15974 Å)[b]		; $f_{n\pi^*}^{(n)}$ = 0.01079; $\boldsymbol{R}_{n\pi^*}^{(n)}$ = ∓0.01442 DBM
$\boldsymbol{m}_{n\pi^*}^{(n)}$	(±0.38759,	∓0.81053, −0.00059 BM)		(projected angle $\angle\boldsymbol{m}_{n\pi^*}$–X-axis = 64.5°)[d]
$\boldsymbol{\mu}_{\pi\pi^*}^{(n)}/e$	(−0.12770,	0.48401, ∓0.01891 Å)[b]		; $f_{\pi\pi^*}^{(n)}$ = 0.18117; $\boldsymbol{R}_{\pi\pi^*}^{(n)}$ = ∓0.03754 DBM
				(projected angle $\angle\boldsymbol{\mu}_{\pi\pi^*}$–$\overline{C'O}$ = −16.2°)[d]
$\boldsymbol{m}_{\pi\pi^*}^{(n)}$	(∓0.01893,	±0.01182, 0.84369 BM)		
$\boldsymbol{\mu}_{n\pi^*,\pi\pi^*}^{(n)}/e = \boldsymbol{\mu}_{\pi\pi^*,n\pi^*}^{(n)}/e$	(0.02042,	0.01578, ∓0.10276 Å)[b]		
$\boldsymbol{\mu}_{n\pi^*,n\pi^*}^{(n)}/e$	(−0.41301,	0.44806, ∓0.04695 Å)[c]		
$\boldsymbol{\mu}_{\pi\pi^*,\pi\pi}^{(n)}/e$	(−0.13881,	1.19746, ∓0.03541 Å)[c]		
$\boldsymbol{\mu}_{00}^{(n)}$	(−2.55363,	4.80145, ∓0.15411 Debye)[c]		

a) Refs. 41, 42, 43, and 46. Regarding the parameterization, see Ref. 1. For $n\pi^*$ and $\pi\pi^*$ transition energies, we use the experimentally assumed values of $\lambda_{g0}^{(n)}$ = 210 nm and 185 nm with the same damping factor $\eta_g^{(n)}$ = 1500 cm^{-1}. b) By the dipole-velocity method. c) The dipole-length method, by which the following results were obtained; $\boldsymbol{\mu}_{n\pi^*}^{(n)}/e$ (−0.01408, −0.00040, ∓0.07319 Å); $f_{n\pi^*}^{(n)}$ = 0.00235; $\boldsymbol{R}_{n\pi^*}^{(n)}$ = ∓0.02445 DBM, $\boldsymbol{\mu}_{\pi\pi^*}^{(n)}/e$ (−0.20961, 0.75493, ∓0.01465 Å); $f_{n\pi^*}^{(n)}$ = 0.44337; $\boldsymbol{R}_{\pi\pi^*}^{(n)}$ = ∓0.00255 DBM (projected angle $\angle\boldsymbol{\mu}_{\pi\pi^*}$–$\overline{C'O}$ = −15.5°), $\boldsymbol{\mu}_{n\pi^*,\pi\pi^*}^{(n)}/e = \boldsymbol{\mu}_{\pi\pi^*,n\pi^*}^{(n)}/e$ (−0.02650, 0.01730, ∓0.07150 Å). Note that diagonal types of moments such as $\boldsymbol{\mu}_{00}^{(n)}$, $\boldsymbol{\mu}_{n\pi^*,n\pi}^{(n)}{}^*$, and $\boldsymbol{\mu}_{\pi\pi^*,\pi\pi^*}^{(n)}$ have no choice except for the dipole-length method. d) An angle measured down from the x-axis of the amide plane; for the $\overline{C'O}$ reference axis, a positive angle is measured toward the N-atom of the amide.

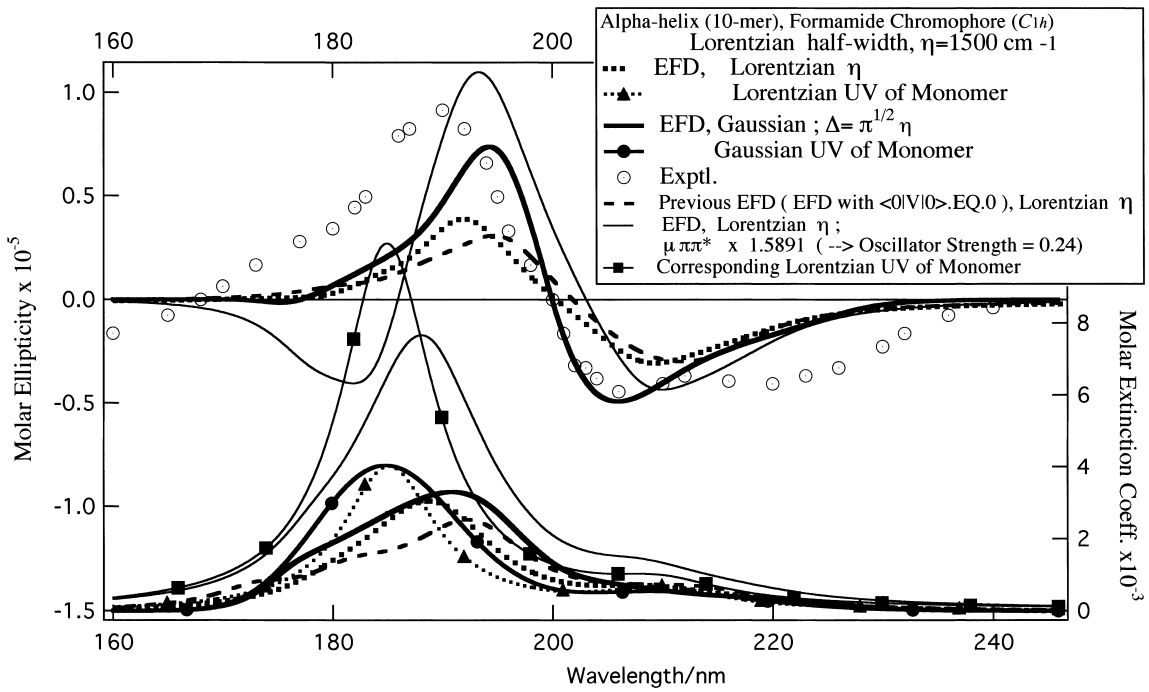

Fig. 3. CD and UV absorption curves for the α-helix of a decapeptide, which were computed with the Lorentzian and Gaussian monomer band shape functions, using the CNDO/S monomer spectroscopic parameters of formamide chromophore (C_{1h}) which were obtained in the dipole-velocity method. The results for previous extended Fano-DeVoe (EFD) method are also plotted.

tively reflected in the CD and UV curves.

α-Helix Structure: We used an idealized right-handed α-helix structure for the backbone dihedral angles[49] $\phi = -57°$, $\psi = -48°$, $\omega = 180°$. In Figs. 3, 4, 5, and 6, the results for the α-helix of decapeptides are shown with the CD curve observed for poly(γ-methyl-*L*-glutamate).[50] In Figs. 3 and 4, we found that the present method exhibits improved CD curves together with the reasonable UV spectral shifts without scaling of V_{mm}^{ff}, which was, however, invoked to obtain reasonable CD and UV bands in the previous method.[1] In Fig. 4, we can see how the

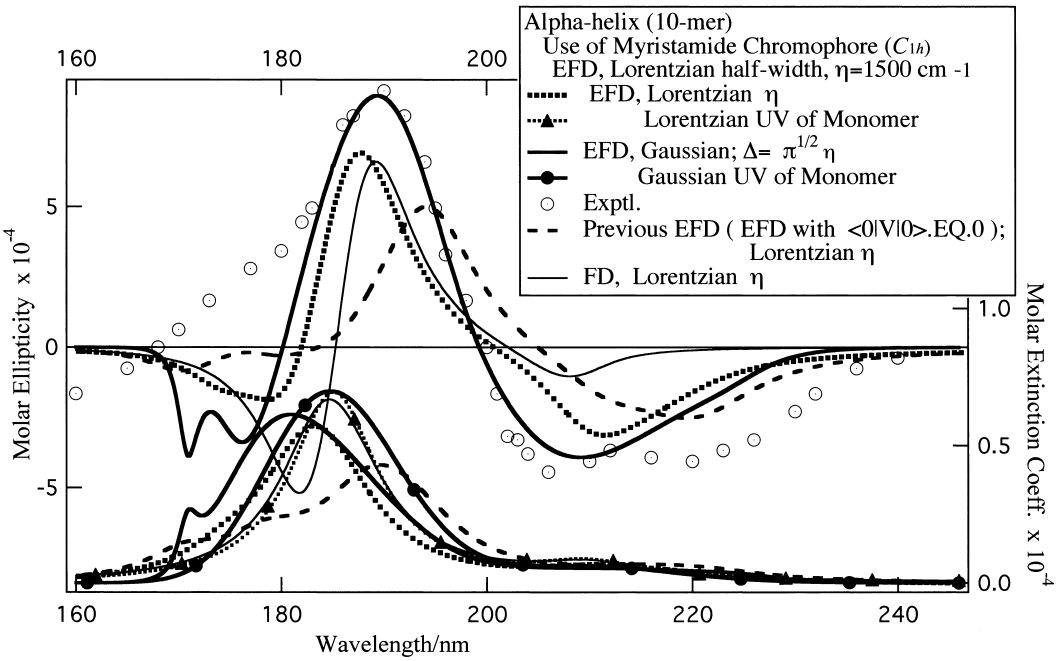

Fig. 4. CD and UV curves for the α-helix of the 10-mer, which were computed with the Lorentzian and Gaussian monomer band shape functions, using the CNDO/S monomer spectroscopic parameters of the conformer *PN* (C_{1h}) of myristamide which were obtained in the dipole-velocity method. The results for previous extended Fano–DeVoe (EFD) method are also plotted.

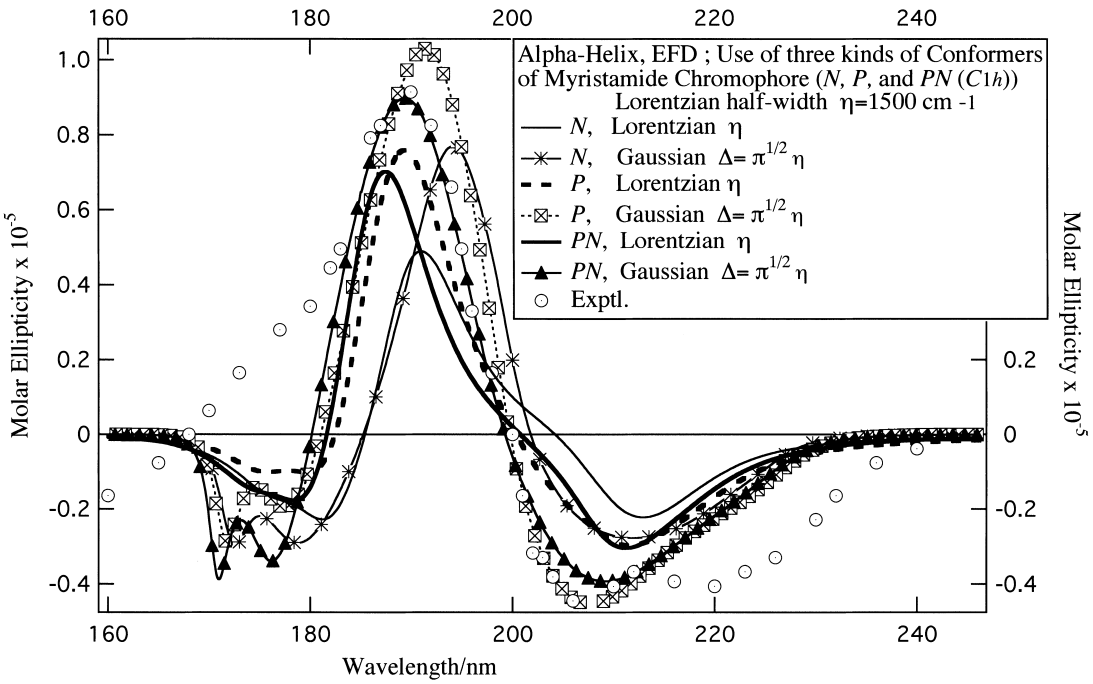

Fig. 5. CD and UV curves for the α-helix of the 10-mer, which were computed with the Lorentzian and Gaussian monomer band shape functions, using the CNDO/S monomer spectroscopic parameters of three kinds of conformers *N*, *P*, and *PN* (C_{1h}) of myristamide which were obtained in the dipole-velocity method.

CD curve obtained by the original Fano–DeVoe method can be refined in the present extended Fano–DeVoe method.

Comparison of Figs. 3, 4, 5, and 6 shows that the CD curves obtained for confomers *P* and *PN* of myristamide with Gaussian band approximation give good agreements with the observed CD spectrum. The achiral formamide leads to poor agreements, owing to much underestimated $\pi\pi^*$ transition moments. As shown in Fig. 3, scaling of the $\pi\pi^*$ transition moment to the experimental oscillator strength of 0.24 gives a reasonable CD curve which is comparable with the results of achiral and chiral conformers of myristamide. This scaling, however, could not produce reasonable CD curves for β-sheet

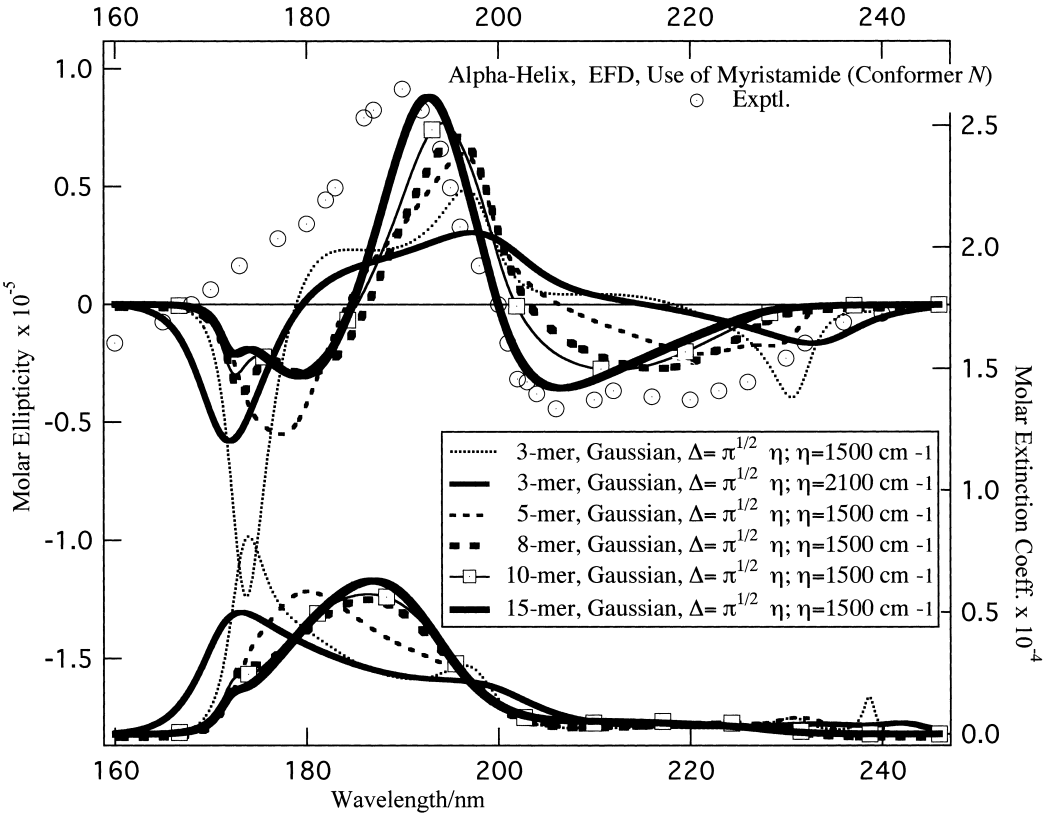

Fig. 6. CD and UV curves of the chain-length dependence for the α-helix polypeptides, which were computed with the Lorentzian and Gaussian monomer band shape functions, using the CNDO/S monomer spectroscopic parameters of the conformer *N* of myristamide which were obtained in the dipole-velocity method.

structures (data not shown). The chain-length dependence examined in Fig. 6 shows a tendency that the CD curves converge on the typical CD curve of α-helix.

The defect of the dipole approximation[51] might not be circumvented especially for small tripeptides, whose molecular sizes fall in the ranges of bond length distances; as shown in Fig. 5, the tripeptides exhibited unusual CD curves when we made use of smaller Gaussian half-widths than $\Delta_g^{(n)} = \sqrt{\pi}\,\eta_{g;L}^{(n)}$ with $\eta_{g;L}^{(n)} = 2100\ \mathrm{cm}^{-1}$. In the Lorentzian approximation, however, we did not observe the unusualness found in Gaussian CD curves which are sensitive to $\Delta_g^{(n)}$ especially for β-sheet structures and small α-helix and β-turn tripeptides. The monopole approximation[51] might become significant in β-sheets and β-turns; in the dipole approximation, the dependence of monomer properties upon CD curves seems to be small for long α-helical polypeptides.

β-Pleated Sheet Strucures: Plotted in Figs. 7 and 8 are the CD and UV bands computed for the antiparallel and parallel β-pleated sheets as two-dimensional puckered arrays of two chains with pentapeptides (2 [chains] $\times$ 5 [peptides]); the CD curve observed for the antiparallel β-sheet is also plotted.[47] These bands were computed using the monomer properties obtained by the dipole-length method for the conformer *N* of myristamide in Table 3. We made use of $\phi = -119°$, $\psi = +113°$, $\omega = 180°$ for parallel β-sheet[49] and of $\phi = -138.6°$, $\psi = +134.7°$, $\omega = -178°$ for the antiparallel β-sheet.[49] We assumed the interchain distances 4.72 Å for two kinds of β-sheets.[7,52]

As shown in Figs. 7 and 8, only the best results for the monomer properties of chiral conformer *N* of myristamide obtained by the dipole-length method were obtained in spite of the use of the experimentally unsatisfactory $\pi\pi^*$ transition directions. In the Gaussian approximation, the experimentally inappropriate $\pi\pi^*$ transition direction seem to bring about unsatisfactorily poor CD and UV band shapes. Compared with the Lorentzian results, one may realize that the $n\pi^*$ UV band having a big hump is relevant to the unusual $n\pi^*$ CD curve in the Gaussian result.

β-Turn Conformations: Using the secular matrix method,[2,5–7] Woody presented the pioneering calculations of various β-turn conformations of tripeptides.[53] Here, we carried out the calculations of CD curves of type I, II, III, and IV β-turn structures for a tripeptide, neglecting side-chain groups; dihedral angles such as ϕ_{i+1}, ψ_{i+1}, (ω_{i+1},) ϕ_{i+2}, ψ_{i+2} (, ω_{i+2}) for type I, II, and III were employed from Ref. 54 (Type I ; $\phi_{i+1} = -60°$, $\psi_{i+1} = -30°$, $\omega_{i+1} = 180°$ and $\phi_{i+2} = -90°$, $\psi_{i+2} = 0°$, $\omega_{i+2} = 180°$, Type III; $\phi_{i+1} = -60°$, $\psi_{i+1} = -30°$, $\omega_{i+1} = 180°$ and $\phi_{i+2} = -60°$, $\psi_{i+2} = -30°$, $\omega_{i+2} = 180°$); those of type IV were employed from No.8 of Ref. 55 (Type IV; $\phi_{i+1} = 120°$, $\psi_{i+1} = 270°$, $\omega_{i+1} = 180°$ and $\phi_{i+2} = 240°$, $\psi_{i+2} = 210°$, $\omega_{i+2} = 180°$). For β-turn tripeptides, we assumed a homo-tripeptide as well. However, for the $\pi\pi^*$ transition energies, we assumed 185 nm for the Gly- and Leu-chromophore and 202 nm for the Pro-chromophore (*trans*-form tertiary amide) following the previous parameterization of Ref. 1.

Shown in Fig. 9 are the CD curves computed using the

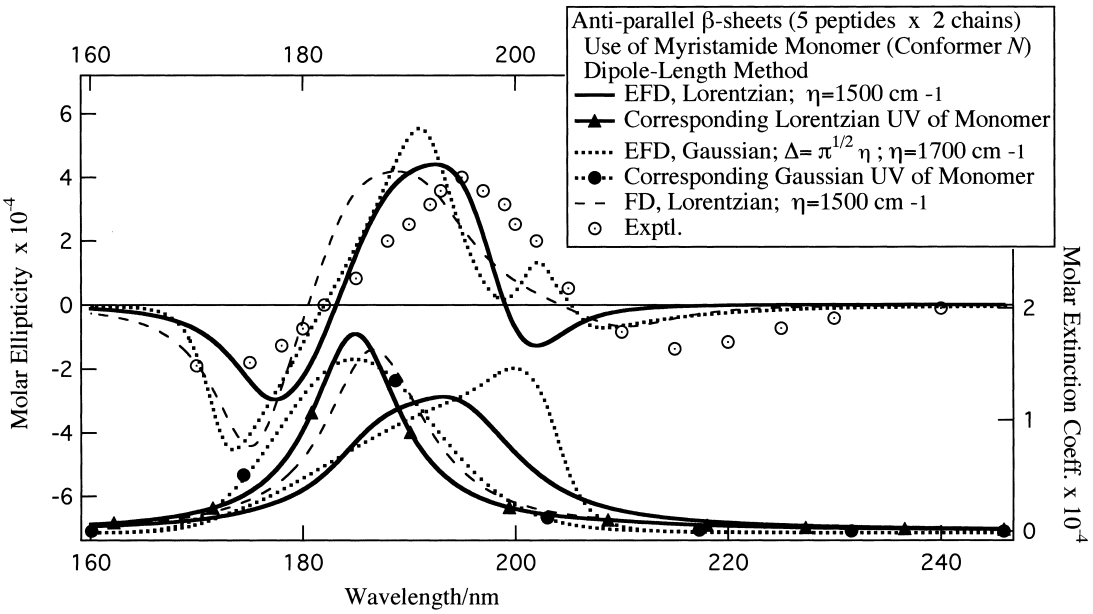

Fig. 7. CD and UV absorption curves for antiparallel β-sheets of 2 (chains) $\times$ 5 (peptides), which were computed with the Lorentzian and Gaussian monomer band shape functions, using the CNDO/S monomer spectroscopic parameters of myristamide which were obtained in the dipole-length method.

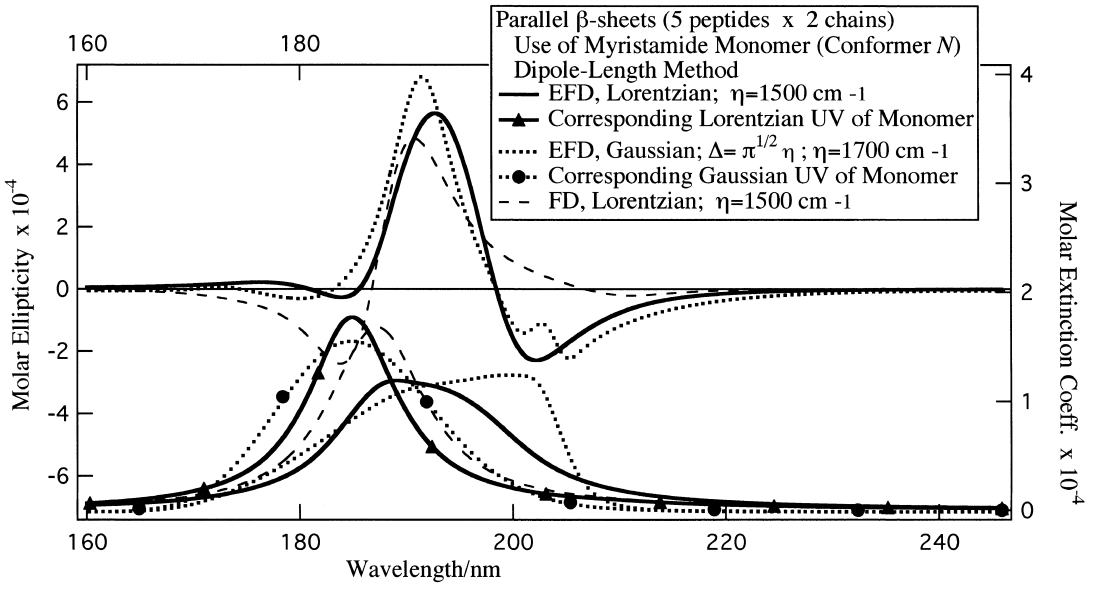

Fig. 8. CD and UV absorption curves for parallel β-sheets of 2 (chains) $\times$ 5 (peptides), which were computed with the Lorentzian and Gaussian monomer band shape functions, using the CNDO/S monomer spectroscopic parameters of myristamide which were obtained in the dipole-length method.

monomer properties of formamide obtained in the dipole-velocity method. For the type II β-turn of Lewis[54] (Type II ; $\phi_{i+1} = -60°$, $\psi_{i+1} = +120°$, $\omega_{i+1} = 180°$ and $\phi_{i+2} = +80°$, $\psi_{i+2} = 0°$, $\omega_{i+2} = 180°$), the CD curve obtained is in good agreement with the CD curve observed for the tripeptide, *N*-acetyl-Pro-Gly-Leu-OH, which is believed to have a 4 $\rightarrow$ 1 hydrogen-bonded type II β-turn conformation.[56] Lorentzian and Gaussian approximations are found to give similar satisfactory results, whereas use of the monomer properties of myristamide gave rise to unsatisfactory results, perhaps due to the large discrepancy of its $\pi\pi^*$ transtion moment direction from the experimental results.[42,43]

In Fig. 9, use of the conformer *N* of myristamide suggests that *N*-acetyl-Pro-Gly-Leu-OH prefers type II′ β-turn structure (the inverse of type II) especially in the Gaussian band approximation. It is, however, difficult to determine which is correct, because CD curves computed for the β-turns as well as the β-sheet structures show extremely sensitive dependence upon monomer spectroscopic parameters compared to the α-helix structure. To conclude this, we must carry out the CD calcula-

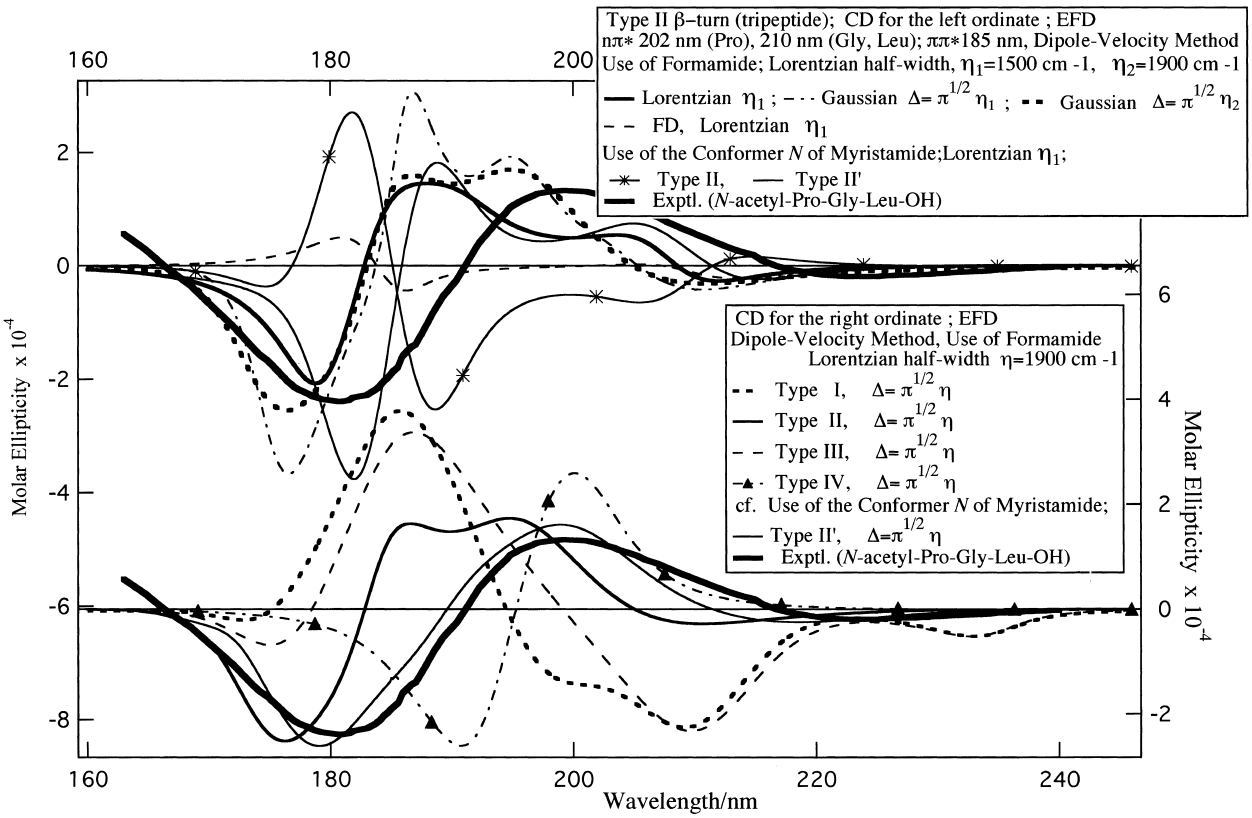

Fig. 9. CD curves for a Type II β-turn of a tripeptide which are plotted in the left ordinate. These CD bands were computed with the Lorentzian and Gaussian monomer band shape functions, using the CNDO/S monomer spectroscopic parameters of formamide which were obtained in the dipole-length method. In the right ordinate, the CD curves for type I, II, III, and IV are plotted. The CD curves computed are compared with the CD curve observed for the tripeptide, *N*-acetyl-Pro-Gly-Leu-OH, supposedly having a $4 \rightarrow 1$ hydrogen-bonded type II β-turn. The results obtained for type II and II′ using the spectroscopic parameters of the conformer *N* of myristamide are also plotted.

tions for huge numbers of possible conformations of β-turn structures gathered by Smith and Pease[57] in their review article which involves Refs. 53, 54, and 55.

3. Final Remarks. (1) The Bayley–Nielsen–Schellman-like matrix theories[2,5–7] involve only the off-diagonal type of *CAE* electrostatic interactions V_{mm}^{fg}. Their successful results[2,5-7] indicate that their wise truncation of the diagonal type of *CAE* interactions V_{mm}^{ff} as well as our stopgap scaling[1] of V_{mm}^{ff} correspond to the present modification of V_{mm}^{ff}. Without the scaling, we have successfully obtained the CD and UV absorption curves. As have qualitatively been shown in Eq. 10, the present success is thought to be brought about by the insertion of appropriately corrected *CAE* energies V_{mm}^{ff} to the denominators of the monomer Green's functions. (2) Based upon the textbook by Eyring et al.,[17] we derived exactly the same CD and UV band shape functions as those of Ref. 1. (3) The present exciton treatment may be extensively applied to cyclodextrin inclusion compounds and nucleic acids, because all the chromophores have permanent dipole moments.[58–60]

References

1 H. Ito, *J. Chem. Phys.*, **111**, 9093 (1999).

2 P. M. Bayley, E. B. Nielsen, and J. A. Schellman, *J. Phys. Chem.*, **73**, 228 (1969).

3 H. Ito and Y. J. I'Haya, *J. Chem. Phys.*, **77**, 6270 (1982).

4 E. U. Condon, W. Altar, and H. Eyring, *J. Chem. Phys.*, **5**, 753 (1937).

5 W. J. Goux and T. M. Hooker, Jr., *J. Am. Chem. Soc.*, **102**, 7080 (1980).

6 N. Sreerama, M. C. Manning, M. E. Powers, J.-X. Zhang, D. P. Goldenberg, and R. W. Woody, *Biochemistry*, **38**, 10814 (1999).

7 E. S. Pysh, *J. Chem. Phys.*, **52**, 472 (1973).

8 J. H. Bene and H. H. Jaffé, *J. Chem. Phys.*, **48**, 1807 (1968).

9 J. H. Bene and H. H. Jaffé, *J. Chem. Phys.*, **48**, 4050 (1968).

10 R. L. Ellis, G. Kuehnlenz, and H. H. Jaffé, *Theor. Chim. Acta (Berl.)*, **26**, 131 (1972).

11 T. N. Misra, *Rev. Pure and Appl. Chem.*, **15**, 39 (1965).

12 A. S. Davydov, "Theory of Molecular Excitons," Plenum, New York (1971), p. 40 and p. 123.

13 R. Kopelman, "Excited States," ed by E. C. Lim, Academic Press, New York (1975),Vol. 2, p. 36 and p. 53.

14 P. J. Stiles , *Nature (London), Phys. Sci*, **232**, 107 (1971).

15 A. D. Buckingham and P. J. Stiles, *Acc. Chem. Res.*, **7**, 258 (1974).

16 H. Ito, Y. Arakawa, and Y. J. I'Haya, *J. Chem. Phys.*, **98**, 8835 (1993).

17 H. Eyring, J. Walter, and G. E. Kimball, "Quantum Chem-

istry," John Wiley & Sons, New York (1944), p. 337.
18 R. Pariser, *J. Chem. Phys.*, **24**, 250 (1956).
19 R. G. Parr, "Quantum Theory of Molecular Electronic Structure," W. A. Benjamin, New York (1963).
20 H. Ito, *J. Chem. Phys.*, **108**, 93 (1998).
21 H. DeVoe, *J. Chem. Phys.*, **41**, 393 (1964).
22 H. DeVoe, *J. Chem. Phys.*, **43**, 3199 (1965).
23 P. W. Atkins, "Molecular Quantum Mechanics 2nd ed," Oxford University Press, Oxford (1983), p. 449.
24 J. Applequist, *J. Chem. Phys.*, **58**, 4251 (1973).
25 E. U. Condon, *Rev. Mod. Phys.*, **9**, 432 (1937).
26 J. A. Schellman, *Acc. Chem. Res.*, **1**, 144 (1968).
27 P. M. Bayley, *Progr. Biophys. Mole. Biol.*, **27**, 1 (1973).
28 H. W. Wyld, "Mathematical Methods for Physics," Addison-Wesley, Reading, Massachusetts (1976), pp. 497–499.
29 D. J. Caldwell and H. Eyring, "The Theory of Optical Activity," Wiley-Interscience, New York (1971), p. 76.
30 F. Eooten, "Optical Properties of Solids," Academic Press, New York (1972), p. 46.
31 R. Loudon, "The Quantm Theory of Light," Clarendon Press, Oxford (1973), p. 61 and p. 84.
32 J. M. Ziman, "Elements of Advanced Quantum Theory," Cambridge University Press (1969), p. 109.
33 W. H. Louisell, "Quantum Statistical Properties of Radiation," John Wiley & Sons, Inc, New York (1973), pp. 313–314.
34 J. A. Schellman, *Chem. Revs.*, **75**, 323 (1975).
35 W. H. Flygare, "Molecular Structure and Dynamics," Prentice-Hall, Inc., Englewood Cliffs, New Jersey (1978), pp. 435–436.
36 J. S. Briggs and A. Herzenberg, *Mole. Phys.*, **21**, 865 (1971).
37 G. E. Forsythe, M. A. Malcolm, and C. B. Moler, "Computer Methods for Mathematical Computations," Prentice-Hall, New Jersey (1977), [Translated into Japanese by Masatake Mori; Kagaku-Gijyutu Publishing Co., Inc., Tokyo (1978), p. 113].
38 L. Z. Stenkamp and E. R. Davidson, *Theor. Chim. Acta (Berlin)*, **44**, 405 (1977).
39 C. Giessner-Prettre and A. Pullman, *Theor. Chim. Acta (Berlin)*, **13**, 265 (1969).
40 R. L. Bowman, M. Kellerman, and W. C. Johnson, Jr., *Biopolymers*, **22**, 1045 (1983).
41 M. B. Robin, "Higher Excited States of Polyatomic Molecules," Academic Press, New York (1975), **Vol. 2**, pp. 122–160.
42 L. B. Clark, *J. Am. Chem. Soc.*, **117**, 7974(1995).
43 D. L. Peterson and W. T. Simpson, *J. Am. Chem. Soc.*, **79**, 2375(1957).
44 A. Volosov, *J. Chem. Phys.*, **87**, 6653(1987).
45 D. W. Urry, *Ann. Rev. Phys. Chem.*, **19**, 477(1968).
46 H. Basch, M. B. Robin, and N. A. Kuebler, *J. Chem. Phys.*, **49**, 5007 (1968).
47 S. Brahms, J. Brahms, G. Spach, and A. Brack, *Proc. Natl. Acad. Sci. USA*, **74**, 3208 (1977).
48 R. W. Woody, *Biopolymers*, **22**, 189(1983).
49 IUPAC-IUB Commission on Biochemical Nomenclature. Abbreviations and Symbols for the Description of the Conformation of Polypeptide Chains. Tentative Rules (1969): *Biochemistry*, **15**, 607 (1970).
50 W. C. Johnson, Jr. and I. Tinoco, Jr., *J. Am. Chem. Soc.*, **94**, 4389 (1972).
51 I. Tinoco, Jr., *Adv. Chem. Phys.*, **4**, 113(1962).
52 K. D. Parker and K. M. Redall, *Nature*, **179**, 905 (1975).
53 R. W. Woody, "Peptides, Polypeptides and Protein," ed by. E. R. Blout, F. A. Bovery, M. Goodman, and N. Lotan, John Wiley, New York (1974), pp. 338–350.
54 P. N. Lewis, F. A. Momany, and H. A. Scheraga, *Biochim. Biophys. Acta*, **303**, 211(1973).
55 C. M. Venkatachalam, *Biopolymers*, **6**, 1425 (1968).
56 S. K. Brahmachari, V. S. Ananthanarayanan, S. Brahms, J. Brahms, R. S. Rapaka, and R. S. Bhatnagar, *Biochem. Biophys. Res. Commun.*, **86**, 605 (1979).
57 J. A. Smith and L. G. Pease, *CRC Crit. Rev. Biochem.*, **8**, 315 (1980).
58 H. DeVoe and I. Tinoco, Jr., *J. Mol. Biol.*, **4**, 500 (1962).
59 R. Rein, *Adv. Quantum Chem.*, **7**, 735 (1975).
60 W. Saenger, "Principles of Nucleic Acid Structure," Springer-Verlag, New York (1984), p. 107.